Electronic Supplementary Information

Diarylethene-Powered Photo-Switching between Precipitated Nanostrips and Dispersed Supramolecular Polymers

Katsuyuki Murai,[a] Honami Matsui,[b] Tatsuya Seki,[a] Takayuki Umakoshi,[b] Christian Ganser,[c] Takashi Kajitani,[d] Sougata Datta,[e] Hiroki Hanayama[f] and Shiki Yagai[*ef]

[a]*Division of Advanced Science and Engineering, Graduate School of Science and Engineering, Chiba University, 1-33 Yayoi-cho, Inage-ku, Chiba 263-8522, Japan.*

[b]*Department of Applied Physics, The University of Osaka, 2-1 Yamadaoka, Suita 565-0817, Japan.*

[c]*Department of Creative Research, Exploratory Research Center on Life and Living Systems, National Institutes of Natural Sciences, Okazaki 444-8787, Japan.*

[d]*Core Facility Center, Research Infrastructure Management Center, Institute of Science Tokyo, 4259 Nagatsuta, Midori-ku, Yokohama 226-8501, Japan.*

[e]*Institute for Advanced Academic Research (IAAR), Chiba University, 1-33 Yayoi-cho, Inage-ku, Chiba 263-8522, Japan.*

[f]*Department of Applied Chemistry and Biotechnology, Graduate School of Engineering, Chiba University, 1-33 Yayoi-cho, Inage-ku, Chiba 263-8522, Japan.*

Corresponding authors:

Shiki Yagai; E-mail: yagai@faculty.chiba-u.jp
Fax: +81-(0)43-290-3401
Tel: +81-(0)43-290-3169

Table of Contents

1. General

Materials and Methods: Column chromatography was performed using spherical neutral silica gel (particle size: 63–210 μm, Kanto Chemical Co. Inc.) or Biotage Flash Purification System Isolera One with Biotage Sfär Silica High Capacity Duo 20 μm, 25 g cartridges. All other commercially available reagents and solvents were of reagent grade and used without further purification. The solvents used for the measurements were either spectroscopic grade or solvents with a purity of at least 95.0%, which were used as received without further purification. Gel permeation chromatography (GPC) was performed with recycling preparative liquid chromatography (LC-9225NEXT, Japan Analytical Industry) equipped with two GPC columns (JAIGEL-2HR Plus and JAIGEL-2.5HR Plus). Molecular mechanics calculations were performed on MacroModel/Maestro version 12.2 (Schrödinger) with OPLS2005 force field without solvent. ^{1}H and ^{13}C NMR spectra were recorded on a Bruker AVANCE III-500M NMR spectrometer, and chemical shifts were reported in parts per million (ppm, δ) and were referenced to the signal of tetramethylsilane (TMS) at 0.00 ppm as internal standard. The resonance multiplicity was described as s (singlet), d (doublet), t (triplet), dd (double doublet), dt (double triplet), and m (multiplet). High-resolution mass spectra were measured on an Orbitrap Exploris 120 (Thermo Fisher Scientific) mass spectrometer using electrospray ionization (ESI). UV/Vis absorption spectra were recorded on a JASCO V760/V660 spectrophotometer equipped with a JASCO ETCS-761 temperature controller using screw-capped quartz cuvettes of 1.0 mm or 1.0 cm pathlengths. Fourier transform infrared (FT-IR) spectra were measured on a JASCO FT/IR-4600 spectrometer using a potassium bromide (KBr) cell with an optical path-length of 1.0 mm and a KBr substrate.

Light-irradiation experiments: Light-irradiation experiments were carried out using a 300-W xenon lamp source (MAX-303) equipped with a band pass filter (HMX290)(λ = 290 nm, 3.4 mW cm^{-2}) for a UV light, and an MLEP-B070W1LR equipped with an MCEP-CR8-070-3 LED lamp (λ = 620–645 nm, 68.8 mW cm^{-2}) for a visible light in dark conditions. Sample solutions in 1.0 cm optical-path-length quartz cuvettes were placed at a distance of 5 mm from the light source.

Scanning electron microscopy (SEM): SEM imaging was carried out using a JEOL JSM-6510 scanning electron microscopy system. Samples were prepared by drop-casting onto Si substrates, dried under vacuum for over 24 h, and then sputtered with Pt using a JEOL JFC-1600 sputter coater.

Atomic force microscopy (AFM): AFM images were obtained under ambient conditions using a Multimode 8 Nanoscope V (Bruker AXS) in PeakForce Tapping (ScanAsyst) mode. The scan rate was set to 0.996 Hz. Silicon cantilevers (SCANASYST-AIR) with a spring constant of 0.4 N/m and a frequency of 70 kHz (nominal value, Bruker, Japan) were used. The samples were prepared by spin-coating (3000 rpm, 1 min) approximately 10 μL of solutions onto freshly cleaved highly oriented pyrolytic graphite (HOPG, 5 mm × 5 mm) substrates at room temperature. AFM images were processed using NanoScope Analysis 3.0 (Bruker).

High-speed AFM (HS-AFM): The custom-built tip-scan HS-AFM system was used in this study, as previously reported[S1]. Micro-cantilevers (AC10DS-A2, Olympus) with a length of ~10 μm were used for high-speed imaging. The micro-cantilevers were fixed on the tip holder of the scanner using nail polish as it was sufficiently resistant to the used organic solvents. The typical resonance frequency was approximately 400 kHz. All HS-AFM imaging was conducted in the tapping mode. The free oscillation amplitude was set to 1−3 nm, and the set-point amplitude was adjusted to 80–90% of the free oscillation amplitude. The feedback gains were adjusted to ensure stable tracking of the sample topography under high-speed conditions. An HOPG substrate (~5 × 5 mm) was adhered to a glass coverslip. The coverslip was fixed on a spin coater. Sample solutions were spin-coated on the HOPG substrate at 3000 rpm for 1 min. For HS-AFM imaging in an organic solvent, a glass cell specifically designed to hold organic solvents was used. The HOPG substrate on the glass coverslip was placed in the glass cell, and HS-AFM imaging was performed in the organic solvent. UV light (Alonefire H42UV, λ = 365 nm, 4.8 mW cm^{-2}) was irradiated from the side of the glass cell during HS-AFM observation.

Powder X-ray diffraction (PXRD): PXRD was measured in a quartz glass capillary with a diameter of 1.5 mm using a Rigaku NANOPIX equipped with a HyPix-6000 (Rigaku) detector. The scattering vector ($q = 4\pi sin\theta/\lambda$), scattering angle θ, and the position of the incident X-ray beam on the detector were calibrated using several orders of layer reflections from silver behenate (d = 58.380 Å), where λ refers to the wavelength of the X-ray beam (Cu $K\alpha$, 1.54 Å). The sample-to-detector distance was 10.0 cm. The obtained diffraction patterns were integrated along the Debye–Scherrer rings to yield 1D intensity data using 2DP software (Rigaku).

Small-angle X-ray scattering (SAXS): SAXS measurements were conducted at BL-10C at the Photon Factory of the High Energy Accelerator Research Organization (KEK) in Tsukuba, Japan. The solvents for all samples were exchanged with *n*-octane. Sample solutions were placed in specialized cells featuring a stainless-steel frame and 20-µm-thick quartz glass windows, with a 1.25-mm optical path-length. Temperature was maintained at room temperature. The experimental setup using X-ray wavelength of 1.5 Å and a sample-detector distance of 1000 mm (calibrated using silver behenate) allowed for a detectable *Q*-range spanning from 0.1 to 5.9 nm^{-1}. Data were collected in 60 frames, each with an exposure time of 10 s. No signs of radiation damage were observed, allowing the frames to be averaged, resulting in a total integration time of 600 s. Scattering data were captured using a DECTRIS PILATUS3 2M detector and subsequently converted from 2D to 1D scattering intensity profiles [*I(Q)* versus *Q*] through radial averaging. The resulting intensity data were normalized with water as a reference standard. The background, attributed to both solvent and cell, was subtracted to yield absolute scattering intensities, reported as *I(Q)* in cm^{-1}. All data reductions were executed using the SAngler software package.

Analysis of SAXS data: Data analysis was carried out with a "core-shell cylinder" model.[S2] (Eq. S1)

$$I_{(q,\alpha)} = \frac{scale}{V_{\text{total}}} F(q,\alpha)^2 \sin(\alpha) + I_{\text{bkg}} \tag{S1}$$

In Eq. S1, α represents the angle between the cylinder axis and the scattering vector q. V_{total} is the total volume of the core-shell cylinder, and "*scale*" corresponds to the volume fraction. I_{bkg} is a flat background. The scattering amplitude $F(q, a)$ is defined as:

$$F(q,\alpha) = (\rho_{\text{c}} - \rho_{\text{s}})V_{\text{c}} \frac{\sin(q\frac{1}{2}L\cos\alpha)}{q\frac{1}{2}L\cos\alpha} \frac{2J_1(qR\sin\alpha)}{qR\sin\alpha}$$

$$+(\rho_{\text{s}} - \rho_{\text{solv}})V_{\text{s}} \frac{\sin(q\left(\frac{1}{2}L + T\right)\cos\alpha)}{q\left(\frac{1}{2}L + T\right)\cos\alpha} \frac{2J_1(q(R+T)\sin\alpha)}{q(R+T)\sin\alpha} \tag{S2}$$

In Eq. S2, V_{c} is the volume of the core, L is the length of the core, R is the radiu
core, T is the thickness of the shell, ρ_{c}, ρ_{s} and ρ_{solv} are the scattering length density of the core, shell and solvent, respectively. The outer radius of the shell is given by $R + T$ and the total length of the outer shell is given by $L + 2T$. J_1 is the first order Bessel function. The scattering length density of the supramolecular polymer and the *n*-octane were set as

$\rho_c = 14.2 \times 10^{-6}$ Å^{-2} and $\rho_s = 8.74 \times 10^{-6}$ Å^{-2} $\rho_{solv} = 6.98 \times 10^{-6}$ Å^{-2}, respectively, which was estimated using SLD calculator tool of SasView software. The "core" was taken to include the DAEc moiety and ester units. The "shell" then comprised the side chain from ethyl spacer to *n*-$C_{12}H_{25}$ chains. The *scale* value was calculated as 5.89×10^{-5} Å^{-2} for c = 300 μM. These values were all fixed in the analysis. Given evidence from AFM measurements, the clear $I(Q) \sim Q^{-1}$ dependency in the dataset persisting throughout the low Q region, L was fixed at 1000 Å (= 100 nm).

2. Synthesis and Characterization

Compound **1** was synthesized according to Scheme S1. Compounds **2**[S3] and **4**[S4] were prepared according to reported procedures.

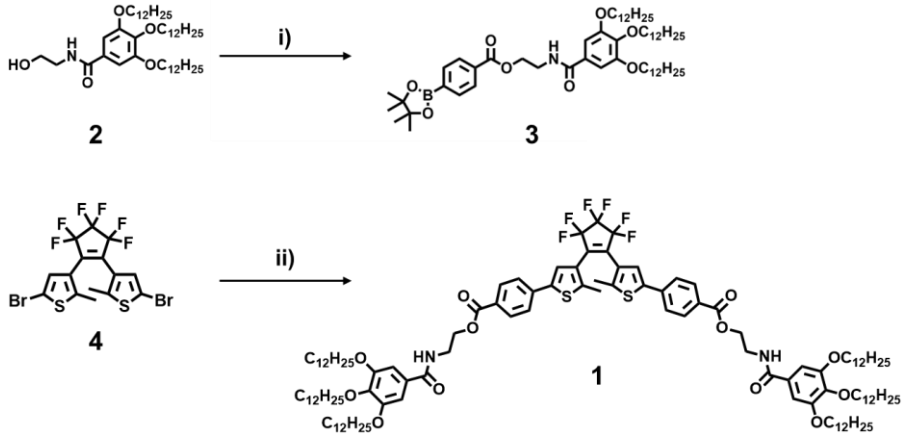

Scheme S1. Synthesis of compound **1**. Reagents and conditions: i) **2**, 4-(4,4,5,5-Tetramethyl-1,3,2-dioxaborolan-2-yl)benzoic acid, *N,N'*-dimethyl-4-aminopyridine (DMAP), 1-(3-dimethylaminopropyl)-3-ethylcarbodiimide hydrochloride (EDC·HCl), CH_2Cl_2, r.t.; ii) **3**, **4**, $Pd(PPh_3)_4$, K_2CO_3, THF, H_2O, 80 °C.

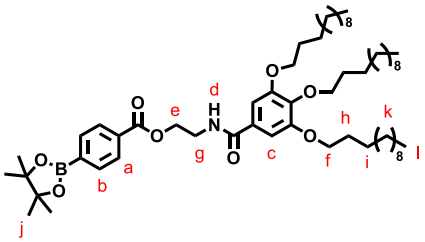

Synthesis and characterization of compound 3: Compound **2** (732 mg, 1.02 mmol), 4-(4,4,5,5-tetramethyl-1,3,2-dioxaborolan-2-yl)benzoic acid (305 mg, 1.23 mmol), DMAP (258 mg, 2.11 mmol), EDC·HCl (590 mg, 3.08 mmol), and dry CH_2Cl_2 (10 mL) were added to a 50 mL two-neck round-bottom flask. The mixture was stirred for 12 h at room temperature. The mixture was diluted with CH_2Cl_2 and washed with water, followed by brine. The organic layer was separated and dried over anhydrous Na_2SO_4, filtered, and evaporated to dryness under reduced pressure. The crude product was purified by column chromatography over silica gel (eluent: ethyl acetate:*n*-hexane = 6:4, v/v) to give compound **3** as a white solid (674 mg, 70% yield).

^{1}H NMR (500 MHz, $CDCl_3$, 20 °C) δ (ppm) = 8.03 (d, J = 8.4 Hz, 2H, PhH_a), 7.88 (d, J = 8.4 Hz, 2H, PhH_b), 6.95 (s, 2H, PhH_c), 6.55 (t, J = 5.6 Hz, 1H, OCONH_d), 4.57 (t, J = 5.3 Hz, 2H, COOCH_e), 4.00–3,96 (m, 6H, OCH_f), 3.84 (dt, J = 5.6 Hz, 5.3 Hz, 2H, CONHCH_g), 1.83–1.70 (m, 6H, CH_h), 1.49–1.43 (m, 6H, CH_i), 1.36 (s, 12H, CH_j), 1.35–1.23 (m, 48H, CH_k), 0.88 (t, J = 7.0 Hz, 9H, CH_l).

^{13}C NMR (125 MHz, $CDCl_3$, 20 °C) δ (ppm) = 167.63, 167.20, 153.11, 141.15, 134.77,

131.82, 129.17, 128.68, 105.56, 84.26, 73.50, 69.26, 67.20, 63.82, 39.93, 31.94, 30.32, 29.75, 29.73, 29.71, 29.59, 29.42, 29.40, 29.38, 29.36, 26.10, 26.08, 24.88, 22.70, 14.11.
HRMS (ESI): *m/z* calcd. for $C_{58}H_{99}O_8NB$ 948.7458 $[M+H]^+$, found 948.7469.

Synthesis and characterization of compound 1: A 100 mL two-neck round-bottom flask was charged with compound **3** (230 mg, 0.24 mmol), 3,3′-(3,3,4,4,5,5-hexafluoro-1-cyclopentene-1,2-diyl)bis[5-bromo-2-methylthiophene] (compound **4**) (58.9 mg, 0.11 mmol) and $Pd(PPh_3)_4$ (23.8 mg, 0.021 mmol) under N_2 atmosphere. A degassed mixture of dry THF (8 mL) and aqueous K_2CO_3 (0.2 M, 2 mL) was added, and the reaction mixture was stirred at 80 °C for 12 h. After cooling to room temperature, the reaction mixture was passed through a small pad of celite column. The filtrate was diluted with ethyl acetate and washed with aqueous HCl (2 M), water, and then brine. The organic layer was separated, dried over anhydrous Na_2SO_4, and evaporated to dryness under reduced pressure. The crude product was purified by column chromatography over silica gel (eluent: ethyl acetate:*n*-hexane = 4:6, v/v) and then by GPC (eluent: $CHCl_3$) to give compound **1** as a white solid (128 mg, 58% yield).

^{1}H NMR (500 MHz, $CDCl_3$, 20 °C) δ (ppm) = 8.05 (d, J = 8.7 Hz, 4H, PhH_a), 7.60 (d, J = 8.7 Hz, 4H, PhH_b), 7.40 (s, 2H, DAE-H_c), 6.96 (s, 4H, PhH_d), 6.55 (t, J = 5.4, 2H, OCONH_e), 4.58 (t, J = 5.3 Hz, 4H, COOCH_f), 4.01–3.96 (m, 12H, OCH_g), 3.86–3.83 (dt, J = 5.4 Hz, 5.3 Hz, 4H, CONHCH_h), 1.98 (s, 6H, DAECH_i), 1.83–1.70 (m, 12H, CH_j), 1.49–1.43 (m, 12H, CH_k), 1.37–1.25 (m, 96H, CH_l), 0.89–0.86 (m, 18H, CH_m).

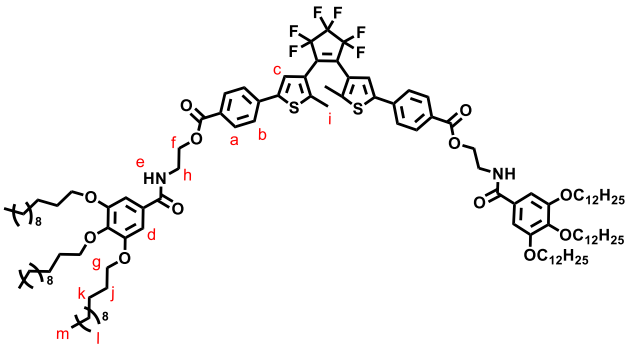

^{13}C NMR (125 MHz, $CDCl_3$, 20 °C) δ (ppm) = 167.64, 166.62, 153.12, 142.91, 141.23, 140.91, 137.78, 130.54, 129.16, 128.80, 126.19, 125.32, 123.88, 105.63, 73.52, 69.32, 63.83, 39.93, 31.95, 31.94, 30.33, 29.75, 29.72, 29.67, 29.60, 29.43, 29.40, 29.38, 26.11, 26.09, 22.70, 14.69, 14.12.
HRMS (ESI): *m/z* calcd. for $C_{119}H_{181}F_6N_2O_{12}S_2$ 2008.2955 $[M+H]^+$, found 2008.2942.

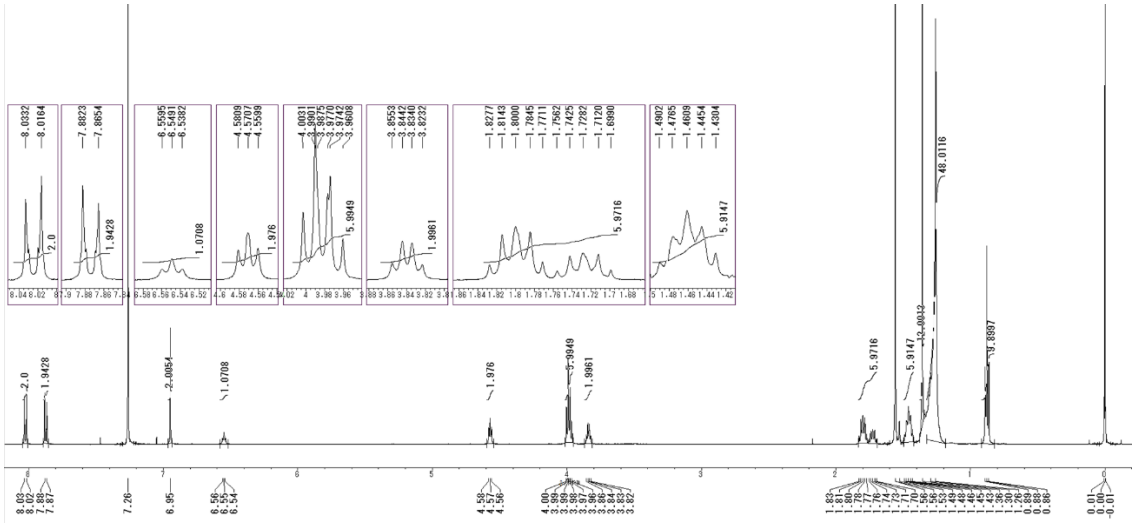

Chart S1. ^{1}H NMR spectrum of compound **3** in $CDCl_3$ at 20 °C.

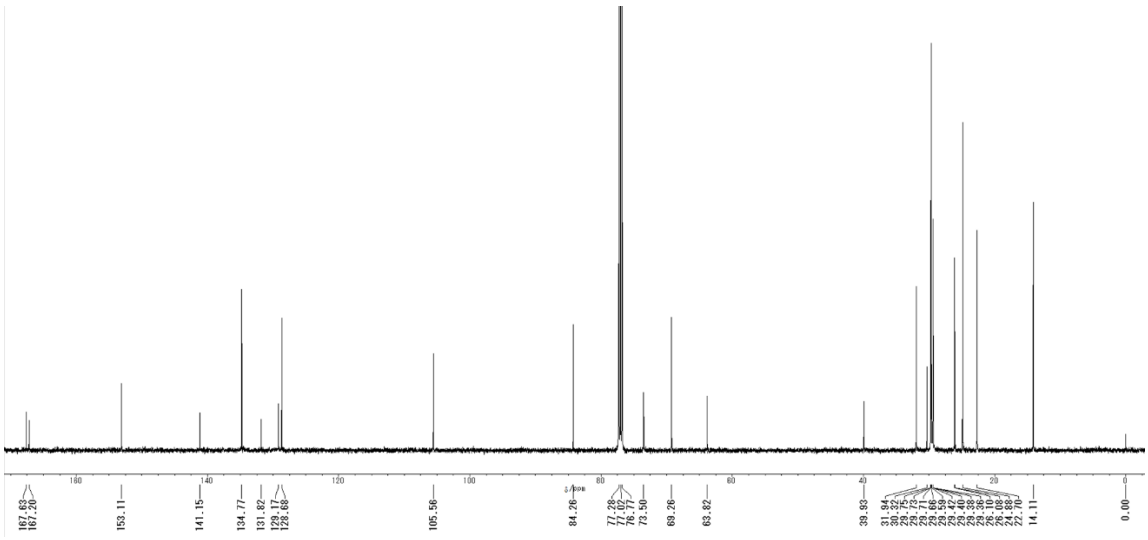

Chart S2. ^{13}C NMR spectrum of compound **3** in $CDCl_3$ at 20 °C.

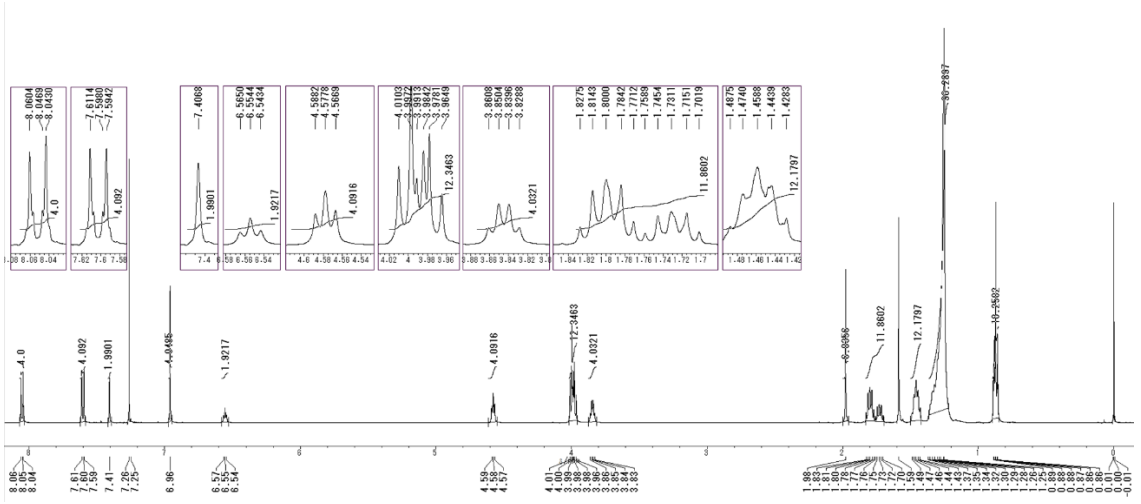

Chart S3. ^{1}H NMR spectrum of compound **1** in $CDCl_3$ at 20 °C.

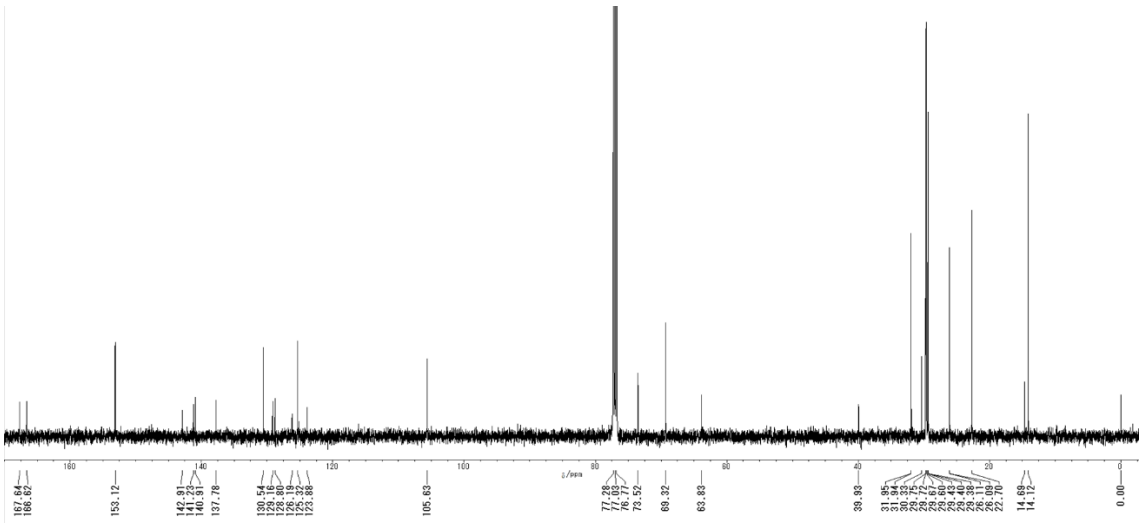

Chart S4. ^{13}C NMR spectrum of compound **1** in $CDCl_3$ at 20 °C.

3. Supporting Figures

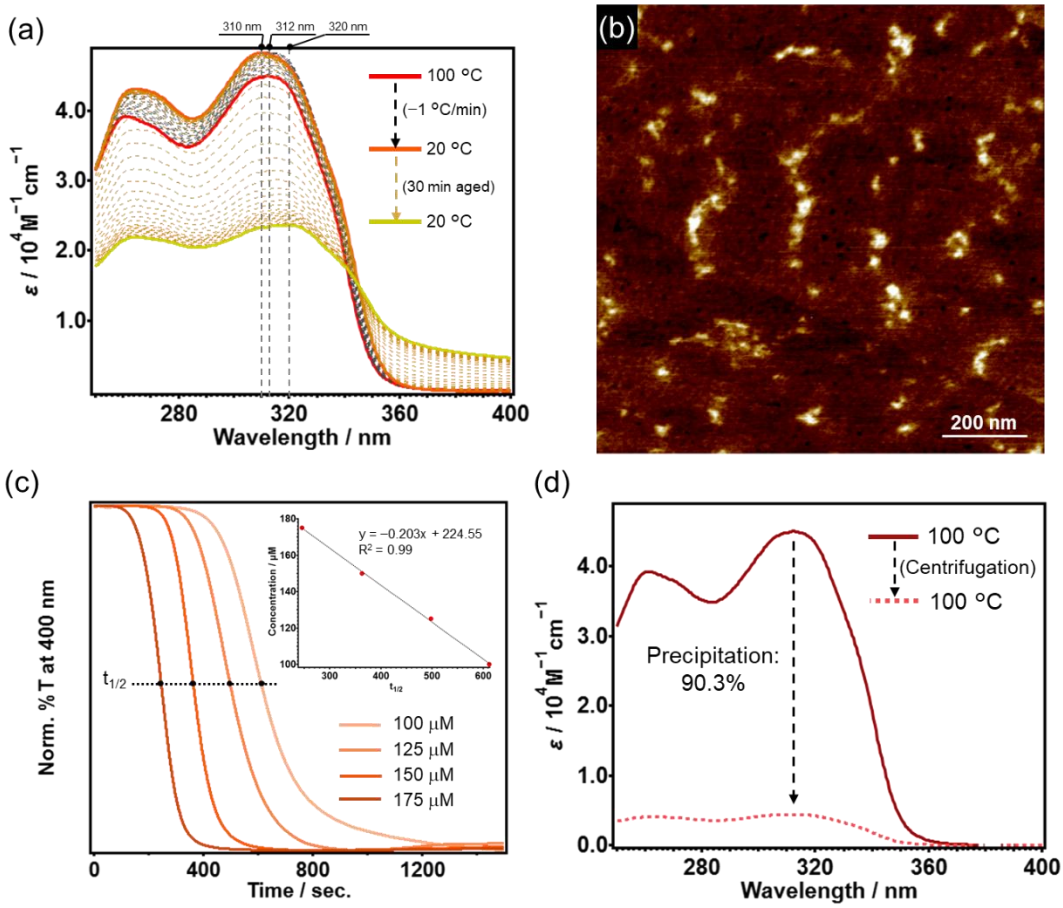

Figure S1. (a) Temperature-dependent changes in the UV-vis absorption spectra of **1o** in *n*-octane/$CHCl_3$ mixture (95:5, v/v; c = 100 μM) upon cooling from 100 °C (red line) to 20 °C (orange line) at a rate of 1.0 °C min^{-1}, followed by standing at 20 °C for 30 min (yellow solid line). (b) AFM image of ill-defined aggregates of **1o** formed immediately after cooling. (c) Time-dependent changes in transmittance at 400 nm upon standing solutions of **1o** at different concentrations. The inset shows a plot of $t_{1/2}$, defined as the time required for the normalized transmittance at 400 nm to decrease to 50%, as a function of concentration. (d) UV/Vis absorption spectra of monomeric **1o** in *n*-octane/$CHCl_3$ mixture (95:5, v/v) at 100 °C before (red solid line) and after (red dashed line) centrifugation (10,000 rpm, 5 min) of the precipitated solution. Based on the decrease in absorbance, more than 90% of **1o** was estimated to form precipitates (c = 100 μM).

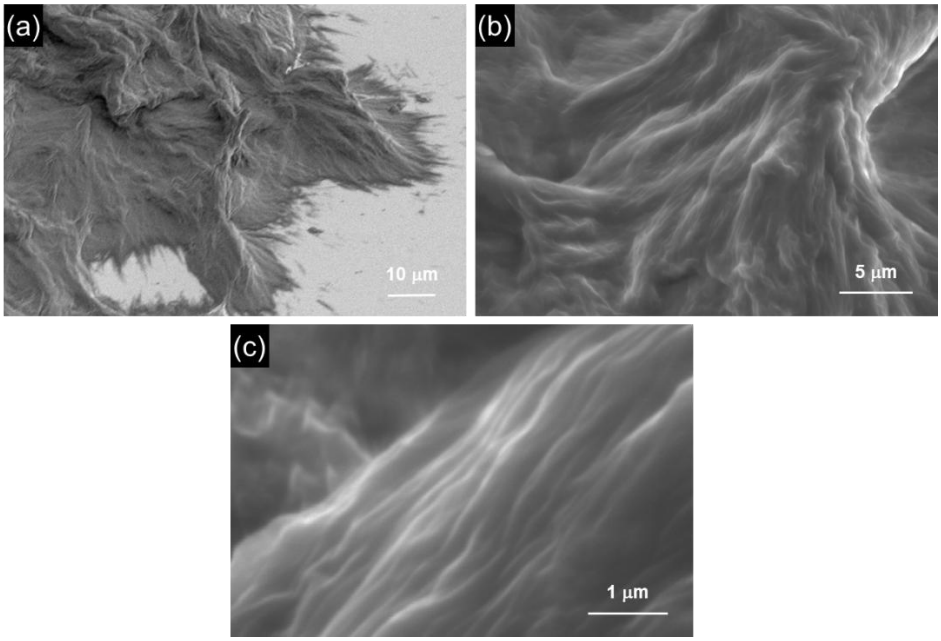

Figure S2. (a–c) SEM images of precipitates composed of **Agg$_{10}$** used for PXRD analysis.

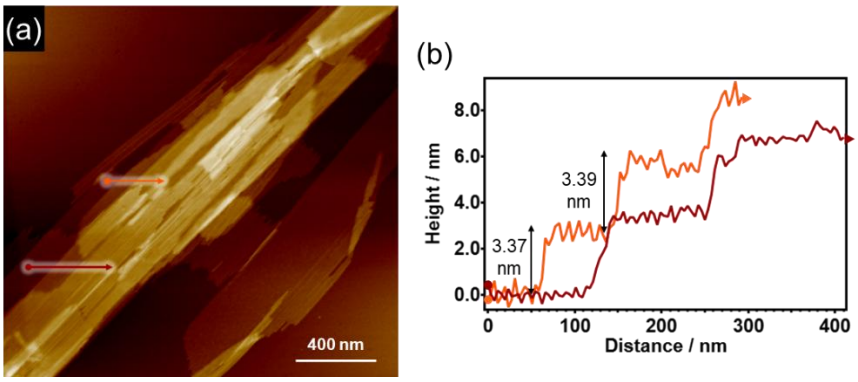

Figure S3. (a) Wide-area AFM image of **Agg$_{10}$**. (b) Cross-sectional analysis along the orange and red arrows in (a), respectively.

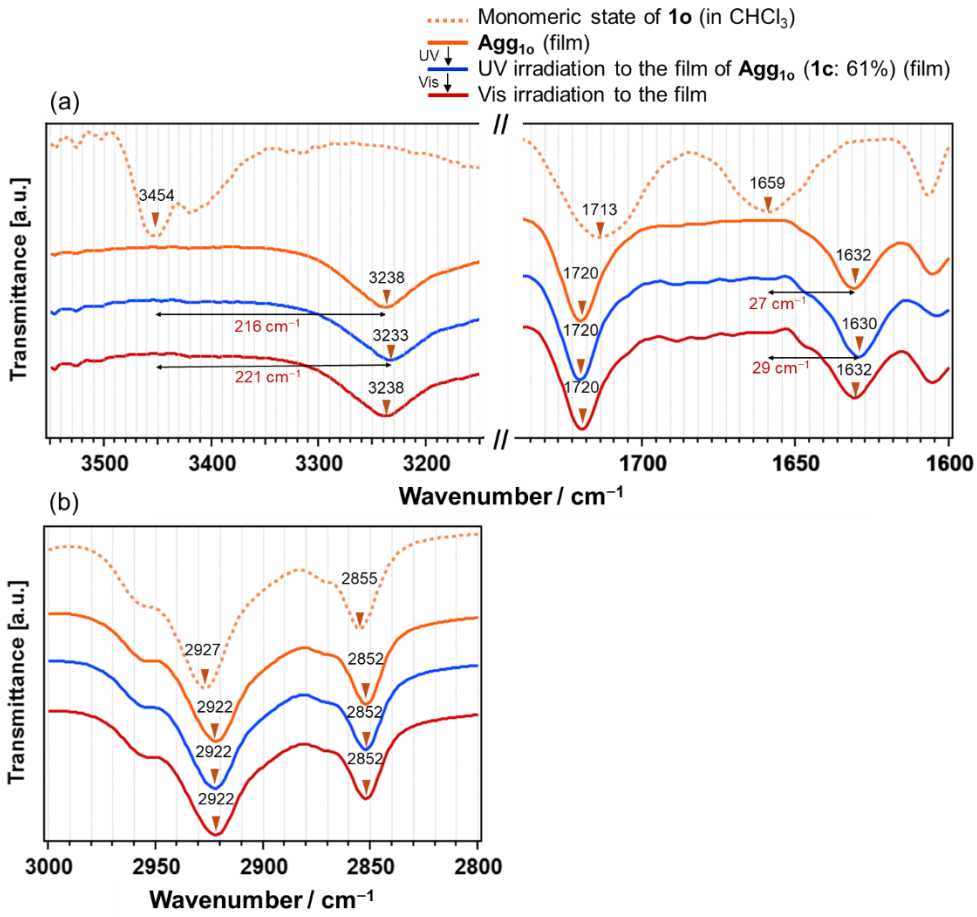

Figure S4. (a,b) FT-IR spectra showing (a) N–H and C=O stretching vibrations and (b) C–H stretching vibrations of monomeric **1o** in $CHCl_3$ (orange dashed line), the film composed of **Agg$_{1o}$** precipitates (orange solid line), the film after direct UV-light irradiation (λ = 290 nm, 5 min; blue solid line), and the film after subsequent visible-light irradiation (λ = 620–645 nm, 5 min, red solid line).

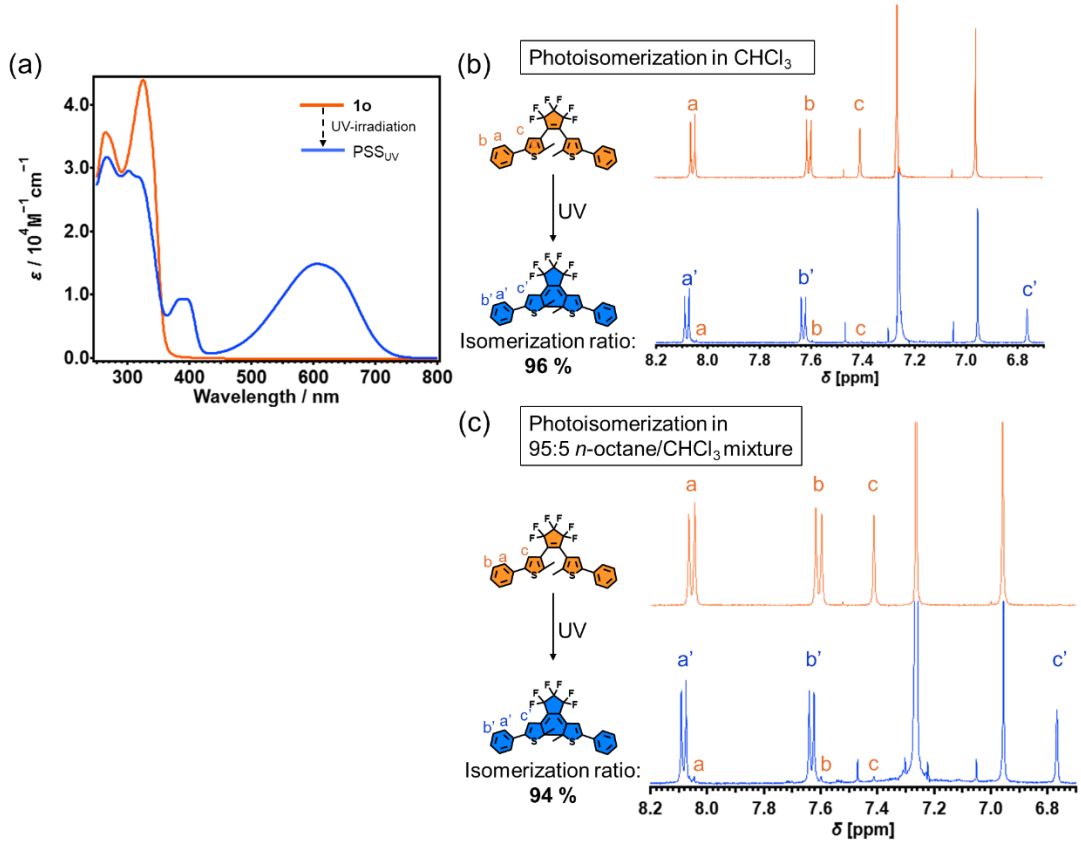

Figure S5. (a) UV/Vis absorption change of a solution of **1o** in $CHCl_3$ (c = 100 µM, orange line) upon UV-light irradiation (λ = 290 nm, 2 min) to reach the photostationary state (PSS, blue line). (b,c) Partial ^{1}H NMR spectra of **1o** in $CDCl_3$ before (orange lines) and after (blue lines) UV-light irradiation, showing photo-isomerization in $CHCl_3$ and in *n*-octane/$CHCl_3$ mixture (95:5, v/v). The samples were prepared by UV-light irradiation of (b) a monomeric **1o** solution in $CHCl_3$ to reach the PSS (**1o**:**1c** = 4:96) and (c) a **Agg$_{1o}$** dispersion in *n*-octane/$CHCl_3$ mixture (95:5, v/v) to reach the PSS (**1o**:**1c** = 6:94).

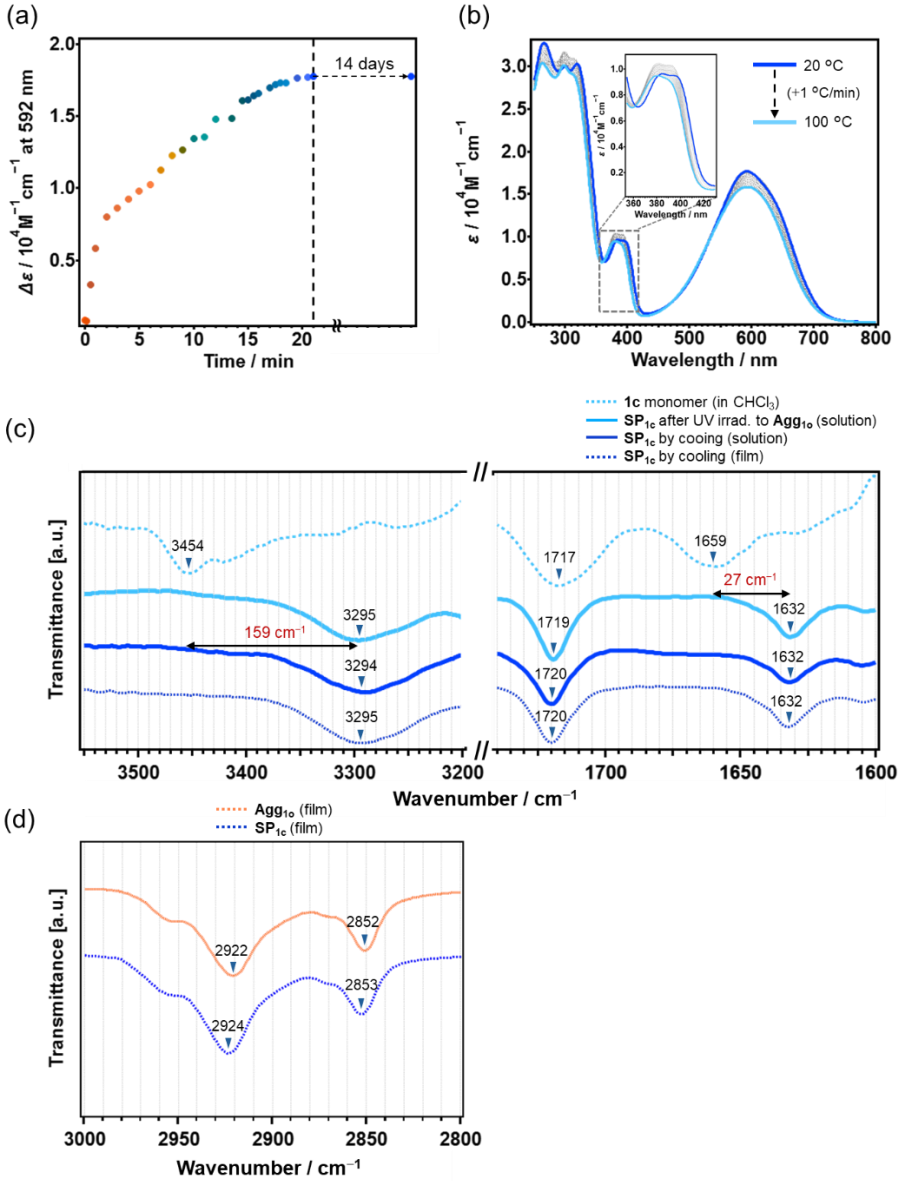

Figure S6. (a) Time-dependent change in the molar absorptivity at 592 nm upon irradiating a solution of **Agg$_{1o}$** (c = 100 μM) in *n*-octane/$CHCl_3$ mixture (95:5, v/v) with UV light for 22 min to reach a PSS_{UV}, and subsequently standing the solution for 14 days. (b) Temperature-dependent changes in UV-vis absorption spectra upon heating the above solution at the PSS_{UV} from 20 °C to 100 °C at a rate of 1.0 °C min^{-1}. (c,d) FT-IR spectra comparing (c) the N–H and C=O stretching vibrations of monomeric **1c** in $CHCl_3$ (light blue dashed line), **SP$_{1c}$** obtained after UV-light irradiation of **Agg$_{1o}$** (light blue solid line) for 22 min in *n*-octane/$CHCl_3$ mixture (95:5, v/v), **SP$_{1c}$** formed by cooling a hot **1c** solution (dark blue solid line) from 100 °C to 20 °C at a rate of 1.0 °C min^{-1} in *n*-octane/$CHCl_3$ mixture (95:5, v/v) and cast film obtained from concentrated **SP$_{1c}$** (dark blue dashed line), and (d) the C–H stretching vibrations of the film composed of **Agg$_{1o}$** precipitates (orange dashed line) and the cast film obtained from concentrated **SP$_{1c}$** (dark blue dashed line).

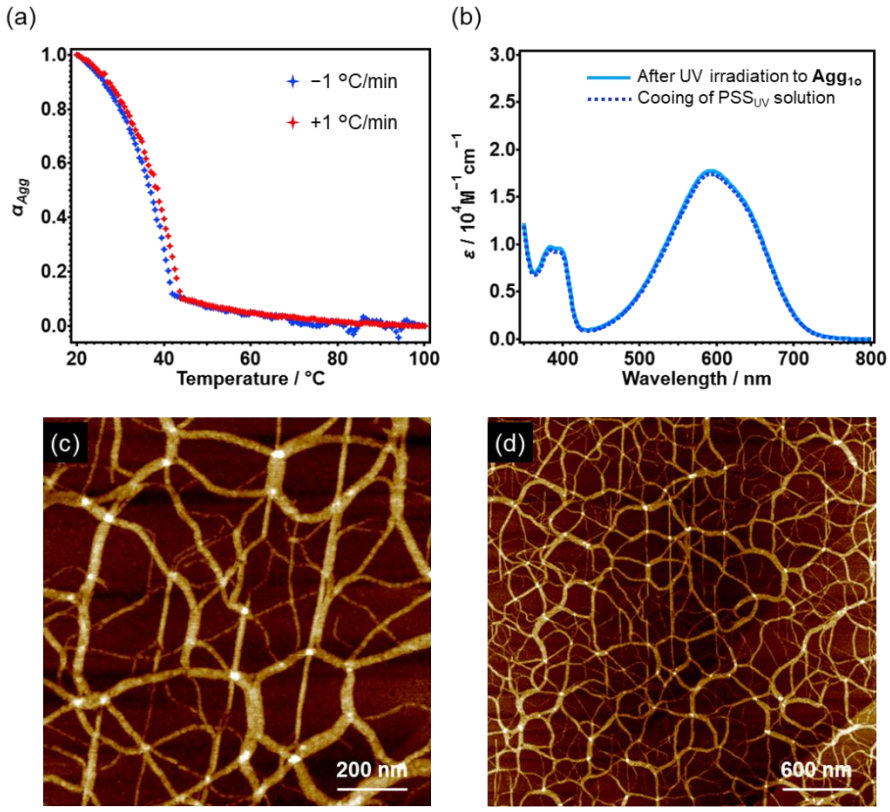

Figure S7. (a) Heating (red) and cooling (blue) curves of **SP1c** formed after UV-light irradiation of a solution of **Agg1o** in *n*-octane/$CHCl_3$ mixture (95:5, v/v; c = 100 μM) for 22 min. The curves were obtained by plotting the fraction of the aggregated molecules, calculated from the absorption change at 415 nm (α_{Agg}), as a function of temperature. (b) Comparison between the UV/Vis absorption spectra of **SP1c** obtained after UV-light irradiation of a solution of **Agg1o** (light blue solid line) and cooling a solution of **1c** (blue dashed line) from 100 °C to 20 °C at a rate of 1 °C min^{-1} in *n*-octane/$CHCl_3$ mixture (95:5, v/v). (c,d) AFM images of **SP1c** obtained by the cooling protocol.

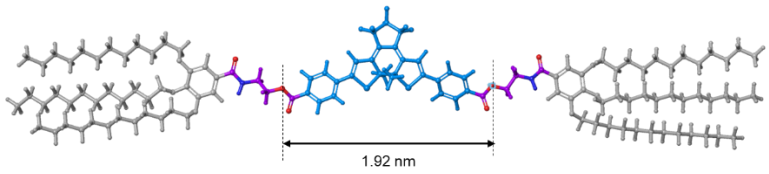

Figure S8. Molecular modelled structure of **1c**.

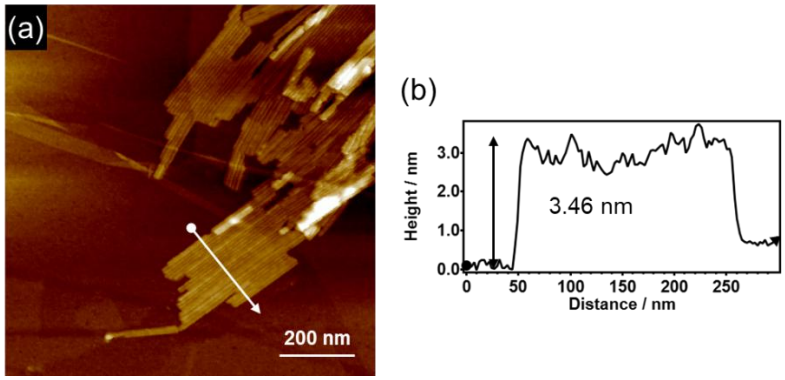

Figure S9. (a) AFM image of **Agg$_{1o}$** sonicated for 8 min. (b) Cross-sectional analysis along a white arrow in (a).

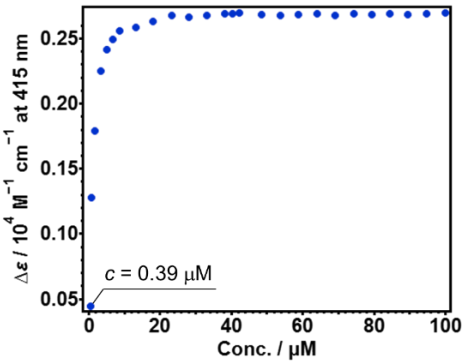

Figure S10. Plots of the molar absorptivity at 415 nm as a function of concentration of **SP$_{1c}$** in *n*-octane.

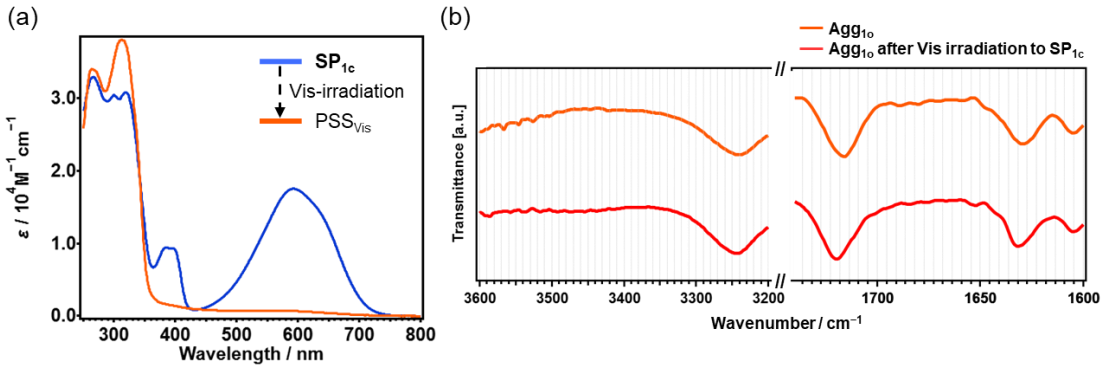

Figure S11. (a) Changes in the UV/Vis absorption spectra of **SP$_{1c}$** (c = 100 μM, blue line) in *n*-octane/$CHCl_3$ mixture (95:5, v/v) upon visible-light irradiation for 11 min to reach a PSS_{Vis} (orange line). (b) FT-IR spectra of **Agg$_{1o}$** (film, orange line) obtained by cooling a solution of **1o** in *n*-octane/$CHCl_3$ mixture (95:5, v/v) from 100 °C to 20 °C at a rate of 1 °C min^{-1}, and **Agg$_{1o}$** (film, red line) formed after irradiating a solution of **SP$_{1c}$** with visible light.

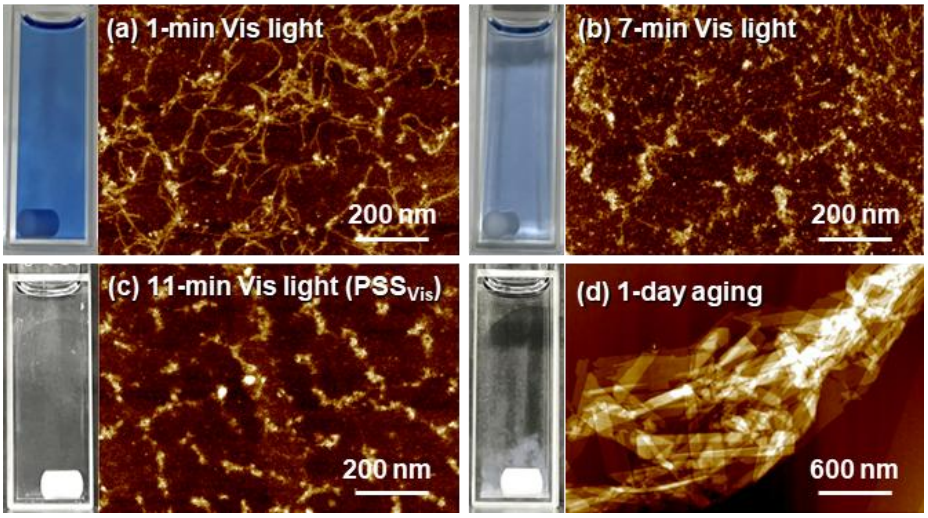

Figure S12. (a–d) Visible-light-induced precipitation of **SP$_{1o}$** and corresponding AFM images of the aggregates. A solution of **SP$_{1c}$** in *n*-octane/$CHCl_3$ mixture (95:5, v/v; c = 100 μM) was irradiated with visible light for (a) 1 min, (b) 7 min, and (c) 11 min (PSS_{Vis}). (d) Images obtained after the irradiated sample was aged for 1 day at 20 °C.

4. Captions for Supporting Movies

Movie S1: HS-AFM movie of **Agg$_{1o}$** in *n*-octane with UV-light irradiation from 60 seconds shown in Figure S3h–k. This movie was captured in a 500 × 500 nm^2 range, 150 ×150 pixels, at 1 fps.

Movie S2: HS-AFM movie of **Agg$_{1o}$** in *n*-octane with UV-light irradiation from 60 seconds, captured in a 750 × 750 nm^2 range, 150 ×150 pixels, at 1 fps.

Movie S3: HS-AFM movie of **Agg$_{1o}$** in *n*-octane with UV-light irradiation from 60 seconds, captured in a 600 × 600 nm^2 range, 150 ×150 pixels, at 1 fps.

Movie S4: HS-AFM movie of **Agg$_{1o}$** in *n*-octane with UV-light irradiation from 80 seconds, captured in an 800 × 800 nm^2 range, 150 ×150 pixels, at 1 fps.

Movie S5: HS-AFM movie of **Agg$_{1o}$** in *n*-octane with UV-light irradiation from 60 seconds, captured in a 700 × 700 nm^2 range, 150 ×150 pixels, at 1 fps.

Movie S6: HS-AFM movie of **SP$_{1c}$** in *n*-octane, captured in a 800 × 800 nm^2 range, 150 ×150 pixels, at 1 fps.

5. Supporting References

S1. H. Matsui, C. Ganser, K. Tamaki, Q. Liu, F.-Y. Chan, T. Uchihashi, P. Verma, Y. Sagara, S. Yagai and T. Umakoshi, *Langmuir*, 2026, **42**, 448–454.

S2. core_shell_cylinder — SasView 6.0.1 documentation, https://www.sasview.org/docs/user/models/core_shell_cylinder.html, (accessed April. 2026).

S3. S. Nagorny, T. Weingartz, J. C. Namyslo, J. Adams and A. Schmidt, *Eur. J. Org. Chem.*, 2023, **26**, e202200996.

S4. R. Kudo, R. Kawai, S. Takamiya, S. Datta, H. Hanayama, N. Hara, H. Tamiaki and S. Yagai, *Chem. Commun.*, 2025, **61**, 8427–8430.